Why Hexagonal Basalt Columns?

Martin Hofmann,[1,*] Robert Anderssohn,[1] Hans-Achim Bahr,[1] Hans-Jürgen Weiß,[1] and Jens Nellesen[2]

[1]*Technische Universität Dresden, Institut für Festkörpermechanik, D-01062 Dresden, Germany*
[2]*RIF e.V.–Institut für Forschung und Transfer, Joseph-von-Fraunhofer-Straße 20, D-44227 Dortmund, Germany*

Basalt columns with their preferably hexagonal cross sections are a fascinating example of pattern formation by crack propagation. Junctions of three propagating crack faces rearrange such that the initial right angles between them tend to approach 120°, which enables the cracks to form a pattern of regular hexagons. To promote understanding of the path on which the ideal configuration can be reached, two periodically repeatable models are presented here involving linear elastic fracture mechanics and applying the principle of maximum energy release rate. They describe the evolution of the crack pattern as a transition from rectangular start configuration to the hexagonal pattern. This is done analytically and by means of three-dimensional finite element simulation. The latter technique reproduces the curved crack path involved in this transition.

Introduction.—The mainly six-sided basalt columns are a fascinating phenomenon of pattern formation. They arise from a network of shrinkage cracks that develop during the cooling of solidified lava. The cooling starts from the top and the cracks follow the temperature field into depth, since thermal shrinkage provides the driving force for the crack propagation.

At the beginning of the process with increasing stresses in the top layer of the solidified lava, secondary cracks meet existing ones at nearly right angles to form so-called T junctions [1]; see Fig. 5 in Ref. [2], compare also Fig. 2(a). The right angles follow from the fact that the traction vector is zero on existing crack faces. In this case an orthogonal crack leads to the highest energy release per crack face through the relief of the in-plane stresses. While the pattern propagates into depth, T junctions change their angles towards 120°, called Y junctions [1].

Additionally, while propagating, the pattern may coarsen by leaving segments of the crack network behind. This phenomenon can be described by fracture mechanics bifurcation analysis, as in Ref. [3]. It is not covered by the present calculations. If the lava lake is deep enough so that the influence of the cooling of the top surface is small compared to possible convective cooling, a steady-state regime with a constant solidification rate establishes [4].

The same preference for hexagonal columns has been found with drying starch slurry [5–7], with repeated drying and moistening of mud, and with freezing and thawing of permafrost soil [8,9]. With increasing number of cycles the crack junctions change from T to Y shape [9].

By visual inspection of a clipped 2D tomographic slice [cf. Fig. 1(a)] extracted from the 3D tomogram of starch slurry dried in a deep dish, the preferred hexagonal shape of the column cross sections becomes obvious; see also a video of the development of column cross sections in Ref. [10]. Further evidence for the hexagonality of the column cross sections is given by image analysis of the tomographic slice utilizing skeletonization: In Fig. 1(b) the relative frequency of the inner angles in convex polygonal representations of column cross sections shows a peak around 120°.

In Ref. [1] it is assumed that the crack pattern junctions change because "joints propagate normal to the direction of local maximum tensile stress and are very responsive to changes of this direction".

It has been shown in Ref. [11] that hexagonal compared to other patterns have lower free Helmholtz energy (involving elastic and fracture energy), assuming equal elastic strain energy and equal cross sectional area. Furthermore, it is stated that a rigorous proof would require finite element calculations.

In Ref. [12] the pattern maturation was modeled by a Voronoi pattern with random starting points, maturing by use of the centers of the polygons as new starting points for
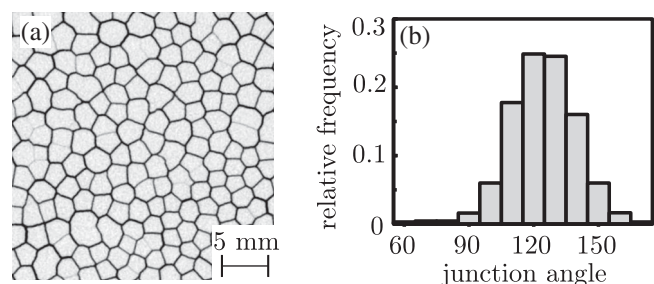
FIG. 1. (a) 2D slice extracted from a 3D tomogram of dried starch slurry columns due to shrinkage crack propagation, showing a tendency towards regular hexagons. (b) Relative frequency of angles in convex polygons of the column cross sections analyzed in the tomogram.

the Voronoi pattern. After some iterations the center points stopped moving, resulting in the matured pattern that agrees well with various field site data.

By energy minimization as in Ref. [11] for a 2D elastic model of the cross sections with respect to the junction points of the pattern starting from a random pattern, Refs. [8,13] showed a tendency toward hexagons. Figure 8 in Ref. [8] shows that matured patterns agree well with the data from basalt columns at various field sites. The only characteristic length of the two models, the ratio of crack face to elastic energy density, provides a too small column diameter of $\approx 10^{-5}$ m for common values of basalt.

So, Ref. [13] stated that the diameter should depend on the characteristic temperature field length, as was shown in Ref. [3] by fracture mechanics bifurcation analysis. There it was shown that the diameter of the columns is determined by the competition of two effects: On the one hand, crack front segments gain more energy by advancing ahead of its neighbors through unloading them, on the other hand, their driving force is reduced as they get into a region of lower thermal shrinkage stress. The influence of the front of the solidifying lava on the diameter was analyzed using a 2D model [14].

Recently, crack pattern formation due to thermal shock has been simulated with a 3D gradient damage model [15] based on Ref. [16]. There the internal length of the gradient model is derived from the critical stress at first occurrence of cracks, which is equivalent to the initial defect length. The calculated final crack pattern is nearly regular, consisting mainly of hexagons. However, the model based on a scalar damage variable cannot describe the stress state close to the crack face so that the interaction between the segments of the crack network is described only approximately, especially at the junctions. Most of the junctions of the simulated pattern even near the starting surface are already close to 120°. T junctions at the start of thermal shock are not considered; thus, the transition from T to Y junctions is not described by Ref. [15].

The observed columns show a tendency towards uniform cross sectional areas with nearly equal crack spacing; see Ref. [10] and Fig. 1(a). This is compatible with the idea that equal spacing reduces mutual unloading.

Also, it is known that among all regular arrays with equal column cross-section area, the hexagonal array is distinguished by its smallest total column surface or crack face area. Hence, with a given amount of energy released by an extension of the array, the energy release rate is highest for the hexagonal array. This is well compatible with the real basalt columns but it does not explain the mechanism by which they develop from a crack array whose junctions are reasonably assumed to be mainly of T shape [1,2]. In reality, the T junctions transform into Y junctions while the crack array is propagating into depth. It is the aim of this Letter to show by means of two periodically repeatable models involving linear elastic fracture mechanics that the

transformation is geometrically possible and mechanically compelling.

Fracture mechanics for driven cracks and the principle of maximum energy release rate.—Since the basalt columns have been brought about by crack propagation, any explanation should somehow involve fracture mechanics. As a basic principle of fracture mechanics, the energy per area A required for creating crack face, called the fracture toughness G_C, must be provided by the energy per area released from the elastic stress field, called the energy release rate G, if the crack is to propagate without external loads:

$$G = -\partial U^{\text{el}}/\partial A = G_C. \tag{1}$$

Here, U^{el} denotes the elastic strain energy.

With Eq. (1) the crack growth increment can be determined but not its direction, because at arbitrary loading the latter deviates from the locally defined crack face plane. Several criteria for the growth direction have been proposed for 2D problems, as, for example, the maximum circumferential stress [17] or minimum strain energy density [18]. As first shown by Ref. [19], for many cases, the criterion of the maximum energy release rate is a suitable one.

In Ref. [20], for cyclic 3D crack propagation, an empirical criterion based on local stress intensity factors was proposed: It introduces two deflection angles, which could lead in general to a discontinuous crack front, also called facets, involving the additional problem of the facet size; see also Ref. [21]. Such discontinuous crack fronts have been observed for high out-of-plane shear loading [22], but not at basalt columns. To avoid this very difficult modeling of a discontinuous crack front, we assume a continuous 3D crack surface, where the crack face increment is described by a local crack extension and a deflection angle with respect to the previous crack plane. These two quantities can vary along the crack front. Using configurational forces in Ref. [23], the crack propagation direction is determined from maximization of the energy release rate of a local crack front extension. This local maximization neglects interaction of crack front segments. Geometrical constraints preclude a propagation of every part of a curved crack front according to the criterion of maximum local energy release rate. Therefore, it is assumed here as a reasonable simplification that every incremental step of crack propagation is governed by the maximum of the energy release rate G_{av} averaged over the crack front [24]:

$$G_{\text{av}} \rightarrow \max. \tag{2}$$

Application to basalt columns with the concept of steady-state energy release rate.—The network of cracks on basalt surfaces is dominated by T junctions [1,2], which may
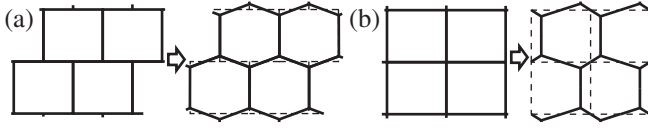
FIG. 2.   Transitions from rectangular to hexagonal periodic arrays: (a) from T to Y junctions and (b) from an X junction to two Y junctions.

FIG. 3.   Scheme of cross section of the unit cell for (a) transition from T to Y and (b) transition from X to Y. (c) Analytically derived normalized energy release rate.

be ideally modeled by a periodic rectangular pattern in Fig. 2(a) as a starting configuration for the transition to the hexagonal pattern with Y junctions. Figure 2(b) shows a transition from a rectangular pattern with so called X junctions and a regular hexagonal pattern. By introducing a new crack segment the X junction turns into two Y junctions.

Let us analyze these transitions with the concept of steady-state energy release rate [25], which implies column growth in a moving steady-state stress field, while the stress field far ahead (I) and far behind (II) the crack front remains unaffected. Hence, one can calculate the energy release rate G without knowing the shape of the crack contour, since during the advance of the crack only a certain volume of the state (I) transforms into the state (II). So G from Eq. (1) can be written as

$$G = -\frac{\partial U^{\mathrm{el}}}{\partial A} = -\frac{dU_{\mathrm{II}}^{\mathrm{el}} - dU_{\mathrm{I}}^{\mathrm{el}}}{dA}. \qquad (3)$$

We here assume homogeneous thermal shrinkage. Ahead of the crack front the material is laterally constrained. According to continuum mechanics the strain energy density can be calculated as $E(\alpha\Delta T)^2/(1-\nu)$. Here E, α, ΔT, and ν denote Young's modulus, thermal expansion coefficient, temperature difference, and Poisson's ratio. Far behind the crack front (II) all stresses are relieved and thus the elastic strain energy is zero. From Eq. (3) for $dV = A_q dz$ and $dA = l_q dz$ we obtain

$$G = \frac{E(\alpha\Delta T)^2}{1-\nu}\frac{A_q}{l_q}, \qquad (4)$$

with A_q being the cross-sectional area and l_q the crack front length in the cross section of the unit cell; see Fig. 3(a) and 3(b). A_q and l_q have to be expressed by x, which is the variable of the transition.

The aspect ratio of the rectangles in Fig. 3(a) has been chosen to $\sqrt{3}/2$ such that the transition into regular hexagons can be performed as easily as possible. (Other rectangles or squares would require more complex constructions.) By Eq. (4) we derive the normalized energy release rate
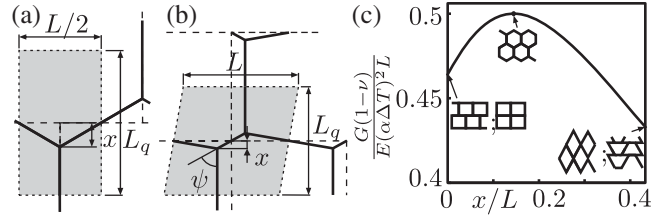
$$\frac{G(1-\nu)}{E(\alpha\Delta T)^2 L} = \frac{\sqrt{3}}{\sqrt{3} - 4(x/L) + 2\sqrt{1 + 16(x/L)^2}}, \qquad (5)$$

depending on the junction point position x; see Fig. 3(a). Equation (5) gives $2\sqrt{3}-3 = 0.464$ for $x = 0$ (T junction) and a value of 0.5 for $x = (\sqrt{3}/12)L$ (Y junction); see Fig. 3(c).

For the transition from X to Y junctions we choose the rectangles as before. Figure 3(b) shows the geometry but now the junction point can laterally move in two directions, described here by x and ψ. The angle ψ is established so that the energy release rate is maximized; hence, $\partial G/\partial\psi = 0$ must hold for a given x, leading to $\tan\psi = L/(4x)$. By this, we obtain the same dependence of G on x as for the transition from T to Y; see Eq. (5).

For both transitions Eq. (5) shows the highest energy release rate for regular hexagons; see Fig. 3(c). The difference in energy release rate between rectangle and hexagon is only 7.2%. This relatively small difference explains why patterns observed in basalt may be not quite regular. This small driving force might not overcome all irregularities. For larger x/L than $\sqrt{3}/12$ G decreases; see Fig. 3(c).

Finite element simulation of the T-Y transition.— Without the restrictions to straight column growth and homogeneous thermal shrinkage, a numerical solution for the proposed transition is found here via iterative finite element (FE) simulation. Stress, strain, and displacement fields, arising from a inhomogeneous temperature field, are calculated by the fundamental equations of linear thermoelasticity using FE software Ansys [26].

The formation of basalt columns with steady-state moving temperature field has been observed in Ref. [4]. By means of fracture mechanics bifurcation analysis for a steady-state temperature field it has been shown in Ref. [3] that the diameter of the columns is inversely proportional to the velocity of the steady-state temperature field and that the difference between effective cooling at the cracks and convective cooling through porosity has a negligible effect on the column diameter. For the sake of simplicity we take a one-dimensional temperature field arising from convection through porosity. In a coordinate system moving in the z direction with the velocity v it can be described by

$$T(\bar{z}) = \begin{cases} T_1 + \Delta T[1 - \exp(-\bar{z}v/D)] & \bar{z} > 0 \\ T_1 & \bar{z} \leq 0 \end{cases}, \quad (6)$$

where D is the thermal diffusivity of the material and $\bar{z}$ belongs to the moving coordinate system. This can also be seen as a simplification of the steady-state temperature model of Ref. [4], with neglected latent heat of the solidifying lava. In the present simulation, curved cracks are supposed to have a negligible effect on the thermal flux and hence on the temperature field as well.

The material parameters are taken from Ref. [3] with $\alpha = 7 \times 10^{-6} \text{ K}^{-1}$, $D = 5 \times 10^{-7} \text{ m}^2/\text{s}$, $E = 57 \times 10^9 \text{ Pa}$, $\nu = 0.21$, $G_C = 84.9 \text{ N/m}$, $T_1 = 100 \,^{\circ}\text{C}$, $L = (1.5–4) \text{ m}$, and $\Delta T = 880 \text{ K}$. According to Ref. [2], $L = 10 \text{ ft} = 3.048 \text{ m}$ is used. The model contains four characteristic lengths: the fracture mechanical length $l_0 = G_C(1 - \nu)/[E(\alpha \Delta T)^2]$, the position of the crack front a_0 in Fig. 4(b) relative to $\bar{z} = 0$ of the moving temperature field [Eq. (6)] at the beginning of the transition, the crack spacing L, and the characteristic length D/v of the temperature field. In this work l_0 and L are directly given and D/v is taken from Fig. 7 in Ref. [3] with $vL/D = 2$ for the bifurcation boundary.

The boundary conditions are shown at a periodically repeatable unit cell in Fig. 4(a), where the modeled part is shaded gray. Symmetry conditions apply at faces **b1** to **b4** as well as at the uncracked part of the boundary faces **c1** and **c3**, while the crack faces at **c1**, **c2**, and **c3** are traction free; compare Fig. 4(b). The boundaries of the 3D FE model in the z direction are chosen to be at $z = \pm 30L$ and are assumed to be traction free. Since the thermal shrinkage far ahead of the crack front is zero and all stresses are relieved far behind the crack front, these boundaries will not influence the result.

Basalt columns show mostly straight striations [27]. This may justify modeling the crack front by straight lines. This is compatible with the computed, only slightly curved crack front for hexagonal columns in Ref. [3]. In this way the tedious numerical calculation of the crack front as in Ref. [3] is avoided and the x and z coordinates of the junction point are the only variables to be determined. They
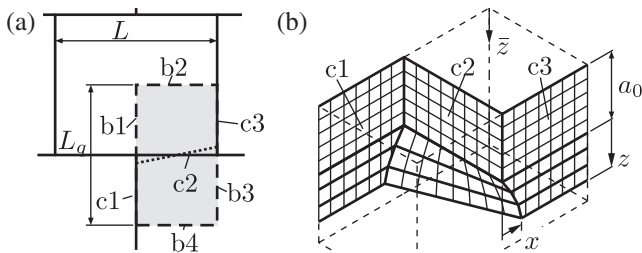
fully describe the crack front of the periodically repeatable configuration.

Figure 4(b) shows how the simulated crack face is extended. A time step Δt leads to a displacement of the temperature field of $v\Delta t$ in the z direction. The junction point coordinates x and z are calculated iteratively for a given time step $\Delta t = L/(100v)$, where Eq. (1) defines the extension of the crack front and Eq. (2) defines the direction of the crack growth for every time step. A check with the time step size $\Delta t = L/(600v)$ produced the same results within numerical precision.

The derivatives for Eq. (1) are calculated by using finite differences with the elastic strain energy and the crack face taken from FE simulations with different crack extensions. For Eq. (2) the derivative of the energy release rate with respect to the extension direction is set to zero, where the derivative is again approximated by finite differences. The direction is given by the angle $\varphi = \arctan(\Delta x/\Delta z)$. The finite differences are kept small compared to the other length of the model, where Δz is chosen in a range of $0.5…1.5v\Delta t$ and Δx is chosen from a variation of the kink angle φ by $\pm 3°$. Only for the initial kink it has been varied in a wide range of $0°$ to $60°$. After every time step the model with the crack front at its new position was remeshed.

An initial kink angle of $\varphi = 43.7°$ at the junction and $a_0 = 2.765L$ are determined from Eqs. (1) and (2) for the first calculation step at an arbitrarily chosen time $t = 0$; see Fig. 4(b). The calculated transition is shown in Fig. 5, where after 50 time steps a final junction angle of $120°$ is obtained. The mesh has been built from hexaeder elements with quadratic shape functions containing 306 000 nodes at the start and 1 150 000 nodes at the end of the simulation of the transition. Tests with a finer mesh showed no effect on the resulting transition. The transition length between the rectangular and the hexagonal pattern appears notably smaller than the crack spacing L. Figure 5 also shows that the normalized elapsed time vt/L is almost proportional to the crack growth in the z direction.

FIG. 4. (a) Top view of a T junction with the FEM model shaded gray. (b) Scheme of crack front extension for the simulation.
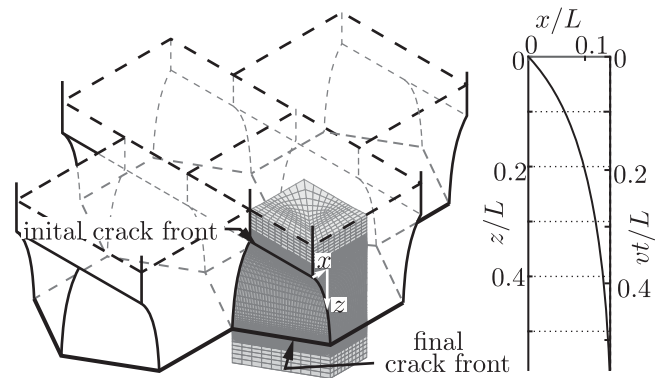
FIG. 5. Calculated transition from the T to Y junction, displaying a cutout ($-0.22 \leq z/L \leq 0.77$) of one-half of the FE model (shaded gray) to show the evolution of the curved crack face against the normalized time vt/L; see also Fig. 4.

Conclusion.—It has been shown here that the principles of fracture mechanics favor the formation of basalt columns with regular hexagons for cross sections.

By starting from a periodic rectangular array, for simplicity, reasons have been given why the crack pattern rearranges itself in the course of crack propagation towards a hexagonal one. Such reorganization is observed with basalt columns [1] and in model experiments with drying starch slurry [7,10]. Rearrangement due to coarsening of the crack mesh, which usually is less conspicuous in basalt, has been clearly demonstrated by computer tomographic analysis of drying slurry [10].

The numerical method applied here might be refined by a less restricted description of the crack front with Fourier series for the crack growth increment and deflection angle. This would lead to more time consuming calculations but also to a more realistic description of the transition. Also, it would be applicable to other 3D fracture mechanical problems with curved crack growth, such as the observed basalt columns with wavy column faces in [28], which are a 3D variant of the observed wavy cracks in glass strips in Ref. [29].

---

[*]Martin.Hofmann@tu-dresden.de

[1] A. Aydin and J. M. DeGraff, Evolution of polygonal fracture patterns in lava flows, Science **239**, 471 (1988).

[2] D. L. Peck and T. Minakami, The formation of columnar joints in the upper part of Kilauean lava lakes Hawaii, Geol. Soc. Am. Bull. **79**, 1151 (1968).

[3] H.-A. Bahr, M. Hofmann, H.-J. Weiss, U. Bahr, G. Fischer, and H. Balke, Diameter of basalt columns derived from fracture mechanics bifurcation analysis, Phys. Rev. E **79**, 056103 (2009).

[4] H. C. Hardee, Solidification in Kilauea Iki lava lake, J. Volcanol. Geotherm. Res. **7**, 211 (1980).

[5] G. Müller, Experimental simulation of basalt columns, J. Volcanol. Geotherm. Res. **86**, 93 (1998).

[6] L. Goehring and S. W. Morris, Order and disorder in columnar joints, Europhys. Lett. **69**, 739 (2005).

[7] H.-A. Crostack, J. Nellesen, G. Fischer, M. Hofmann, H.-G. Rademacher, and W. Tillmann, Analysis of crack patterns in drying corn starch by in-situ radiography and x-ray computer tomography, Exp. Mech. **52**, 917 (2012).

[8] E. A. Jagla and A. G. Rojo, Sequential fragmentation: The origin of columnar quasihexagonal patterns, Phys. Rev. E **65**, 026203 (2002).

[9] L. Goehring, Evolving fracture patterns: columnar joints, mud cracks, and polygonal terrain, Phil. Trans. R. Soc. A, **371** (2013), 20120353.

[10] H.-A. Crostack *et al.*, http://www.lwt.mb.tu-dortmund .de/pub.php?file=Scaling_of_Columnar_.Joints_in_Starch -Experiment_EE, 03 2010.

[11] Z. P. Bazant and L. Cedolin, *Stability of Structures: Elastic, Inelastic, Fracture and Damage Theories* (Oxford University Press, New York, 1991).

[12] P. Budkewitsch and P.-Y. Robin, Modelling the evolution of columnar joints, J. Volcanol. Geotherm. Res. **59**, 219 (1994).

[13] E. A. Jagla, Maturation of crack patterns, Phys. Rev. E **69**, 056212 (2004).

[14] M. Hofmann, H.-A. Bahr, H.-J. Weiss, U. Bahr, and H. Balke, Spacing of crack patterns driven by steady-state cooling or drying and influenced by a solidification boundary, Phys. Rev. E **83**, 036104 (2011).

[15] B. Bourdin, J.-J. Marigo, C. Maurini, and P. Sicsic, Morphogenesis and Propagation of Complex Cracks Induced by Thermal Shocks, Phys. Rev. Lett. **112**, 014301 (2014).

[16] B. Bourdin, G. A. Francfort, and J.-J. Marigo, The variational approach to fracture, J. Elast. **91**, 5 (2008).

[17] F. Erdogan and G. E. Sih, On the crack extension in plates under plane loading and transverse shear, J. Basic Eng. **85**, 519 (1963).

[18] G. C. Sih, Strain-energy-density factor applied to mixed mode crack problems, Int. J. Fract. **10**, 305 (1974).

[19] M. A. Hussain, S. L. Pu, and J. Underwood, Strain energy release rate for a crack under combined mode I and II, ASTM STP **560**, 2 (1974).

[20] M. Schöllmann, H. A. Richard, G. Kullmer, and M. Fulland, A new criterion for the prediction of crack development in multiaxially loaded structures, Int. J. Fract. **117**, 129 (2002).

[21] A. Pons and A. Karma, Helical crack-front instability in mixed-mode fracture, Nature (London) **464**, 85 (2010).

[22] F.-G. Buchholz, A. Cherguib, and H. A. Richard, Fracture analyses and experimental results of crack growth under general mixed mode loading conditions, Eng. Fract. Mech. **71**, 455 (2004).

[23] E. Gürses and C. Miehe, A computational framework of three-dimensional configurational-force-driven brittle crack propagation, Comput. Methods Appl. Mech. Eng. **198**, 1413 (2009).

[24] V. Lazarus, J.-B. Leblond, and S.-E. Mouchrif, Crack front rotation and segmentation in mixed mode I + III or I + II + III, Part II: Comparison with experiments, J. Mech. Phys. Solids **49**, 1421 (2001).

[25] J. W. Hutchinson and Z. Suo, Mixed mode cracking in layered materials, Adv. Appl. Mech. **29**, 63 (1992).

[26] Ansys 15 user manual, 2013.

[27] M. P. Ryan and C. G. Sammis, Cyclic fracture mechanisms in cooling basalt, Geol. Soc. Am. Bull. **89**, 1295 (1978).

[28] L. Goehring and S. W. Morris, Scaling of columnar joints in basalt, J. Geophys. Res. **113**, B10203 (2008).

[29] A. Yuse and M. Sano, Transition between crack patterns in quenched glass plates, Nature (London) **362**, 329 (1993).